

From quasi-static to dense flow regime in compressed frictional granular media.

Florent Gimbert* and David Amitrano
*Institut des Sciences de la Terre, CNRS-Université Joseph Fourier, Grenoble,
FRANCE, 1381 rue de la Piscine, BP 53, 38041 Grenoble Cedex 9*

Jérôme Weiss
*Laboratoire de Glaciologie et de Géophysique de l'Environnement,
CNRS-Université Joseph Fourier, Grenoble, FRANCE,
54 rue Molière, BP 96, F-38402 Saint-Martin d'Hères Cedex*

Gaël Combe
*UJF-Grenoble 1, Grenoble-INP, CNRS UMR 5521,
3SR Lab., B.P. 53, F-38041 Grenoble Cedex 09, FRANCE*
(Dated: June 15, 2022)

We investigate the evolution of multi-scale mechanical properties towards the macroscopic mechanical instability in frictional granular media under compressive loading. Spatial correlations of shear stress redistribution following nucleating contact sliding events and shear strain localization are investigated. We report growing correlation lengths associated to both shear stress and shear strain fields that diverge simultaneously as approaching the transition to a dense flow regime. This shows that the transition from quasi static to dense flow regime can be interpreted as a critical phase transition. Our analysis does not show any characteristic shear band thickness potentially formed at the onset of instability.

The mechanical behavior of granular materials is of wide concern, from natural hazard in geological context to engineering application. However, the evolution of properties towards the flowing instability is still partially understood. Within packings of spheres, heterogeneous distributions of contact forces on a scale much larger than the typical particle size [1] may control the mechanical response of the granular assembly, characterized by long range correlations and collective motions [2]. The concept of jamming [3] provides a powerful framework to analyse the onset of granular flows. Large efforts have been done in this direction by considering assemblies of non frictional particles, which exhibit jammed states resisting small stresses without irreversible deformation, whereas unjammed systems flow under any applied stresses [3]. As granular materials play a fundamental role in geophysical instabilities (e.g. granular gouges within fault zones, landslides), the concept of jamming might be a powerful tool to investigate these problems. However, two more ingredients are of primary importance in those cases. First, frictional granular materials have to be considered, leading to changes in the physics of jamming: the packing fraction is not a pertinent parameter anymore and the transition from an unjammed to a jammed state is rather controlled by the non-rattler fraction [4, 5]. Secondly, the loading conditions drastically differ from the one commonly used to study jamming, since, rather than performed at constant volume, a confining pressure has to be considered. In that case, the non-rattler fraction is not allowed to evolve freely and a percolating strong force network remains in the flowing phase, called the dense flow regime [6].

Here we consider compression tests under multi-axial loading: an increase of the axial stress σ_1 is prescribed whereas the 2D confining pressure σ_3 is kept constant. These multi-axial conditions correspond to the generic case encountered in the Earth and the stress control avoids stress relaxations and associated feedbacks, i.e. the stress and strain localization structures develop freely. Experiments [7] and theoretical works [8] have been conducted in this configuration on either continuous or discrete materials. In continuous materials, the macroscopic instability has been first tackled by the use of bifurcation theory, which considers a transition from an homogeneous to an heterogeneous deformation field materialized by the creation of a perennial macroscopic shear band spanning the whole sample [8, 9]. Within granular materials, either in experiments or simulations, computing the deformation field over a large macroscopic strain window, those perennial shear bands appear and seem to show characteristic sizes [7, 10]. However, this vision is counterbalanced by the heterogeneous and long range correlated kinematics of quasi-static granular flow [2]: at which temporal and spatial scales and at which stage of the loading can we consider the granular assembly to deform homogeneously? What are the relevant key features of the deformation and stress fields associated to the onset of instability?

We use the Molecular Dynamics discrete element method to perform our simulations [11]. Two-dimensional granular assemblies made of frictional circular grains are considered. The grains surfaces are uniformly distributed, setting the largest grain diameter D_{max} such that $D_{max} = 3D_{min}$. Periodic boundary

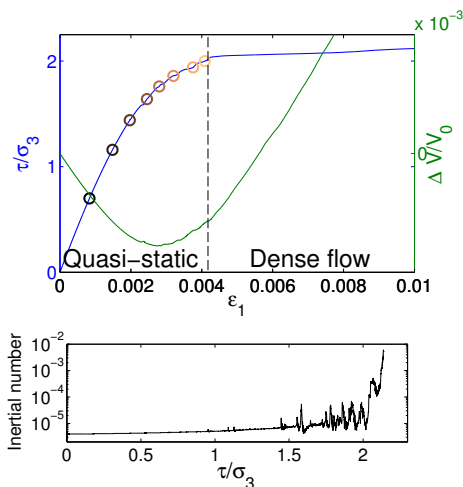


FIG. 1. Macroscopic behavior of a sample made of 10000 grains during compressional testing. Top : Deviatoric stress $\tau/\sigma_3 = (\sigma_1 - \sigma_3)/\sigma_3$ (blue line) and macroscopic volume variation $\Delta V/V_0$ (green line) as a function of axial deformation. Color dots correspond to locations where coarse-graining analyses of Figures 3(Top) and 4(Top) are performed. Bottom : Inertial number I as a function of the imposed deviatoric stress τ .

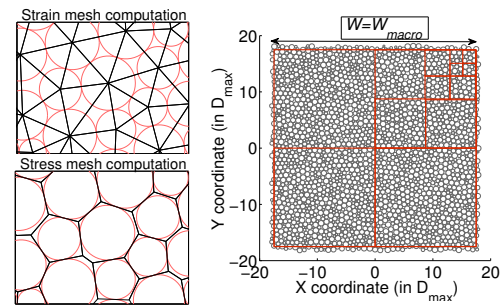


FIG. 2. Left: Delaunay (top) and modified Voronoi (bottom) tessellations for a polydisperse granular material. Right: Coarse graining analysis on a 2500 grains sample.

conditions are used [11]. Grains interact via linear elastic laws and Coulomb friction when they are in contact [12]. Dense and highly coordinated initial packings, characterized by a porosity $\eta_i \approx 0.15$ and a coordination number $z_i \approx 4$, are obtained by isotropic frictionless compression of dilute grains sets. We focus in this study on compression tests, setting the particle friction to $\mu_{micro} = 1$. The confining pressure σ_3 is sized by setting the contact stiffness $\kappa = k_n/\sigma_3$ equal to 1000 [11], where k_n is the normal contact stiffness coefficient. The vertical stress σ_1 is increased at constant rate. To characterize sample size effects [10], we performed 320 simulations on 2500 grains samples, 80 simulations of 10000 grains and 20 simulations of 45000 grains. Most of the results presented here concern 10000 grains samples. Whatever the sample size, we used a stress increment $\delta\sigma_1^t$ equal to $1.10^{-6} \times \sigma_3$ at each discretisation time interval $t_r = \sqrt{\frac{m_{min}}{\times k_n}}/25$, where m_{min} is the mass of the lighter grain. This leads to an inertial number I [11] of the order of $10^{-6} - 10^{-5}$ at the initial stage of the test (Figure 1), which ensures quasi-static conditions.

Figure 1(a) shows a typical macroscopic stress-strain curve. An initial contracting phase is observed, only because of an elastic contact between particles [13], until a peak of contraction is reached, after which the sample dilates continuously. The deviatoric stress $\tau = \sigma_1 - \sigma_3$ reaches a plateau at values slightly larger than $2\sigma_3$, obtained for values of axial strain ϵ_1 of about 0.004. Before this specific point, while undergoing brutal increase during plastic avalanches, the inertial number I remains lower than 10^{-4} (Figure 1(b)), which is often considered

as the upper bound for quasi-static conditions [11, 14]. This region corresponds to the quasi-static regime. On the reverse, at values of τ greater than $\tau_c = 2\sigma_3$, that corresponds to a macroscopic friction $\mu_{macro} \sim 0.5$, a brutal increase of I of several orders of magnitude is observed, reaching values of the order of 10^{-2} , which corresponds to a transition toward a dense flow regime, where inertia comes into play. At this transition, stress concentrations resulting from cooperative effects are expected, triggering preferential weak zones where flow is favoured. In the case of our samples made of circular grains, this leads to a softening of the whole granular assembly and thus to a macroscopic friction much smaller than μ_{micro} . According to this, studying the spatial structure of both stress and strain fields is a key point to understand the mechanisms that generate the macroscopic instability. We thus focus, in this study, on the “dynamics” of the granular assembly, i.e. on the response of the granular assembly to a small stress increment in terms of associated stress concentration and strain localization structures that form during mechanical loading.

We first characterize the spatial extent of stress concentrations within the granular sample by means of a coarse graining analysis [15, 16] : an averaged shear stress rate $\langle \dot{\tau} \rangle$ [17] is computed at different stages of mechanical testing (cf color dots on Figure 1) over a time window T and over a broad range of spatial scales L , from the micro-scale corresponding to the scale of the mesh element, to the macroscale corresponding to sample size (Figure 2). For a given assembly of grains, the components of the stress tensor are computed as $\sigma_{ij} = \frac{1}{V} \sum_g \sum_c (r^c - r^g) f_g^c$ [18], where V is the surface associated to the grain assembly, that corresponds to the sum of surfaces associated to each grain including the amount of porosity calculated using the modified Voronoi tessellation (Figure 2), f_g^c is the contact force exerted on grain g at contact c , r^c is the position of c , and r^g is the position of the center of g . Considering two successive configurations, the stress rate tensor is obtained by differentiating the respective stress tensor components in time. The time resolution used is $T = \sqrt{N_g} \times 100 \times t_r$,

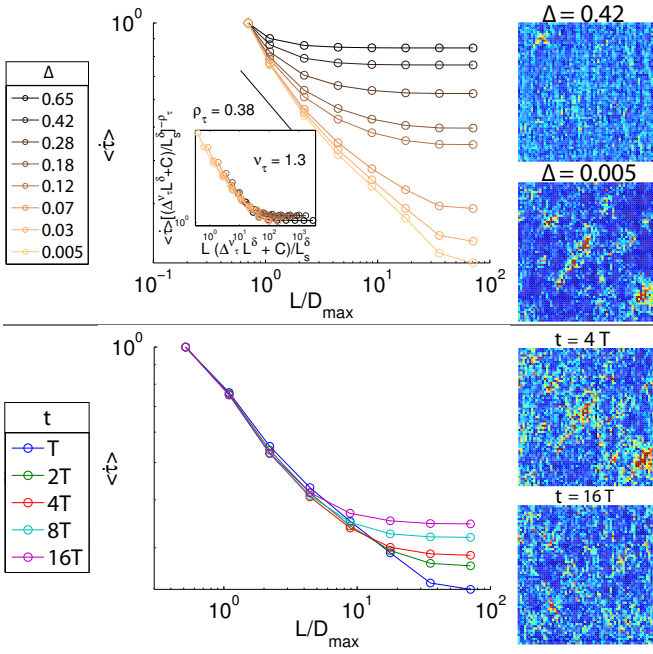


FIG. 3. Multi-scale analysis performed on the shear stress rate field $\dot{\gamma}$. A selection of corresponding fields is shown on the right. Top: $\langle \dot{\gamma} \rangle$ versus L for decreasing values of Δ . Configuration locations on the stress-strain curve are shown on Figure 1. The timescale T is used to compute values of $\langle \dot{\gamma} \rangle$. The inset displays data collapse with respect to Δ (equation 1). We find $\nu_{\tau} = 1.3$, $C = 0.5$ and $\delta = 1$. Bottom: $\langle \dot{\gamma} \rangle$ versus L at $\Delta = 0.005$ when increasing the timescale t from $t = T$ to $t = 16T$. For graphical convenience, all computed values have been normalized by the ones computed at the micro-scale.

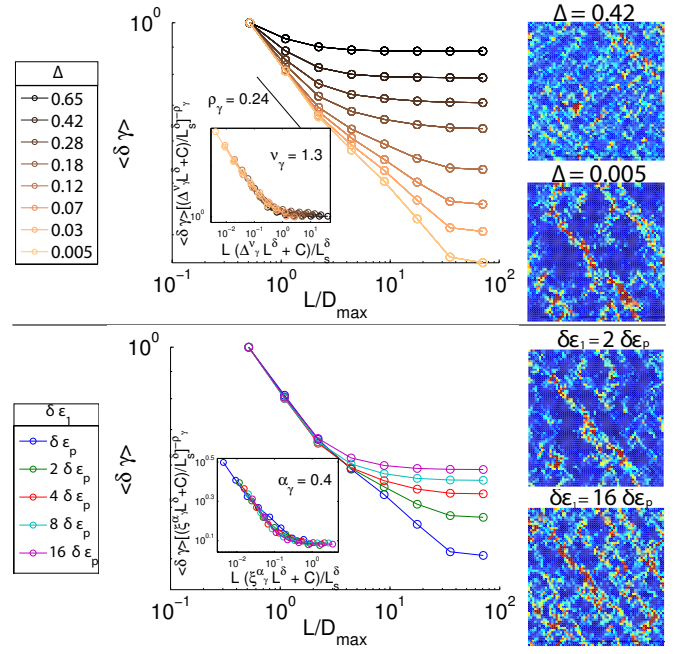


FIG. 4. Multi-scale analysis performed on the incremental shear strain field $\delta\gamma$. A selection of corresponding fields is shown on the right. Top: $\langle \delta\gamma \rangle$ versus L for decreasing values of Δ towards the critical point. The deformation scale $\delta\epsilon_1 = \delta\epsilon_p = 1.10^{-5}$, consistent with the susceptibility analysis presented on Figure 5, is used to compute values of $\langle \delta\gamma \rangle$. The inset displays data collapse with respect to Δ (equation 1). We find $\nu_{\gamma} = 1.3$, $C = 0.5$ and $\delta = 1$. Bottom: $\langle \delta\gamma \rangle$ versus L at $\Delta = 0.005$ when increasing $\delta\epsilon_1$ from $\delta\epsilon_1 = \delta\epsilon_p$ to $\delta\epsilon_1 = 32\delta\epsilon_p$. The inset displays data collapse with respect to $\xi = \frac{\delta\epsilon_1 - \delta\epsilon_p}{\delta\epsilon_p}$. We find $\alpha_{\gamma} = 0.4$. For graphical convenience, all computed values have been normalized by the ones computed at the micro-scale.

where N_g is the number of grains of the sample. This timescale corresponds to the travel time of elastic waves through the granular assembly [10]. Results are shown on Figure 3 (Top), from the early stages of biaxial testing up to $\tau_c = 2\sigma_3$. At the early stages of macroscopic deformation, a decrease of $\langle \dot{\gamma} \rangle$ with L is observed at small scales while for L -values larger than a crossover scale l_{τ}^* a plateau is observed. This means that shear stress rate fields are heterogeneous for $l \ll l_{\tau}^*$, and homogeneous for $l \gg l_{\tau}^*$. Hence, l_{τ}^* is the associated correlation length [16]. As macroscopic deformation proceeds, l_{τ}^* grows until reaching the entire size of the system at τ_c where a power law scaling $\langle \dot{\gamma} \rangle \sim L^{-\rho_{\tau}}$ is observed, with $\rho_{\tau} = 0.38$. The cut-off remaining on the scaling at $\Delta \rightarrow 0$, where $\Delta = \frac{\tau_c - \tau}{\tau_c}$ is the control parameter, is a finite size effect [10]. These results suggest a progressive structuring of the stress field as approaching the transition to the dense flow regime, associated to the divergence of the correlation length l_{τ}^* . It can be verified from a collapse analysis (inset of Figure 3(Top)) that l_{τ}^* diverges as

$$l_{\tau}^* \sim \frac{L_s^{\delta}}{\Delta^{\nu_{\tau}} L_s^{\delta} + C}. \quad (1)$$

where $\nu_{\tau} = 1.3 \pm 0.1$ is the divergence exponent. Parameters δ and C characterize the finite size effect. A similar analysis performed on other moments $\langle \dot{\gamma}^q \rangle$ of the shear rate [10] confirms the divergence of l_{τ}^* at $\Delta \rightarrow 0$, and reveals their multi-fractality at the critical point. As stated previously, these particular features of the shear stress field are observed at a specific timescale $t = T$ corresponding to the elastic waves travel time. This multi-scale behaviour is no longer observed at larger timescales (Figure 3(Bottom)), as a clear departure from power law is observed for $t > T$. Hence, the multi-scale properties of the shear stress rate field are only observed at the time of propagation of the elastic information throughout the sample. Beyond this time, a decorrelation is observed, explained by the superposition in time of several uncorrelated events, consistent with a correlated stress structure associated with little memory, limited to the elastic wave travel time.

To study whether similar observations can be reported on the shear strain field, we consider a delaunay triangulation performed on the grain centers (Figure 2), af-

ter having removed the rattlers grains from the grain set, that allows to compute the partial derivatives at the mesh scale as $\epsilon_{ij} = 1/2(\partial u_i/\partial x_j + \partial u_j/\partial x_i)$, where (u_1, u_2) and (x_1, x_2) are respectively the incremental displacements and spatial coordinates of grain centers. Our coarse graining analysis is then performed by averaging partial derivatives at various scales, similarly to (author?) [15, 16]. An average shear strain rate [17] is thus obtained as a function of L . While not shown here, if one uses the constant timescale T to compute incremental displacements, a divergence of the correlation length associated with the shear strain rate field is not observed. Thus, the structure of the total strain field does not form simultaneously to the stress field, by means of long-ranged elastic interactions. Intuitively, this would be the case if one would consider only the elastic component of the strain. Here, for $N_g = 10000$, $\sim 10^4$ stress increments are prescribed during the propagation time of an elastic wave throughout the sample. Hence, a multitude of contacts, in our case about 5% of the whole contact network, are then sliding, although elastic interactions didn't have time to travel across the entire sample, i.e. we are not in conditions of infinitely slow driving that could be obtained using event-driven algorithms [11]. Despite this, a progressive structuring of the shear strain field is observed by considering constant macroscopic deformation windows $\delta\epsilon_1 = \delta\epsilon_p = 1.10^{-5}$ to compute the scaling of $\langle \delta\gamma \rangle$ (Figure 4). A divergence of the correlation length l_γ^* similar to the one observed on the shear stress rate field is obtained as approaching the transition to the dense flow regime, as we find $\nu_\gamma = \nu_\tau = 1.3$ from a collapse analysis (equation 1). When considering larger macroscopic deformation windows, the multi-scale properties of the deformation field are no longer observed, pointing out that $\delta\epsilon_1 = \delta\epsilon_p$ is a characteristic value. As the material softens when τ increases, the corresponding time of integration decreases as the critical point is approached. This corresponding time can either be smaller or larger than the elastic wave traveling time T , depending on the imposed loading rate $\delta\sigma_1^{\dot{r}}$. However, whatever the loading rate considered and the size of the system, $\delta\epsilon_1 = \delta\epsilon_p$ remains equal to 1.10^{-5} , pointing out that a given amount of plastic activity has to operate in order to observe multi-scale properties within the incremental shear strain field. As the correlation lengths l_τ^* and l_γ^* diverge the same way, this plastic activity is probably the direct consequence of the progressive structuring of the stress field.

An understanding of the characteristic value $\delta\epsilon_p$ can be obtained from a four-point dynamic susceptibility χ_4 [19, 20] analysis on the inter-particles contact network. From a contact configuration that we refer as “initial”, selected at a value of axial deformation denoted ϵ_1^{init} , we compute the self-overlap order parameter $Q_{\epsilon_1^{init}}(\delta\epsilon_1) = \frac{1}{N_c} \sum_{i=1}^{N_c} w_i$, where N_c is the number of contacts that are not sliding in the initial configuration

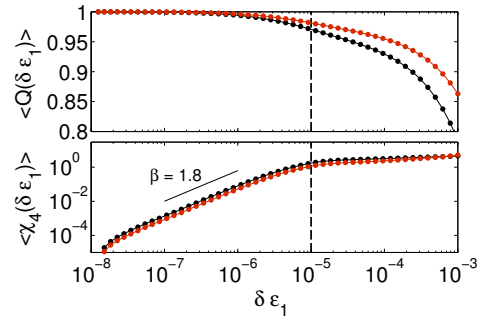


FIG. 5. Susceptibility analysis performed in the quasi-static phase on the sliding contacts taking part of the major (red curves) and minor (black curves) network. Top: Averaged self-overlap order parameter $\langle Q(\delta\epsilon_1) \rangle$. Bottom: Corresponding four-point average susceptibility $\langle \chi_4(\delta\epsilon_1) \rangle$. The vertical dashed line indicates the deformation value $\delta\epsilon_p = 1.10^{-5}$, where a change of behavior is observed.

and w_i is a step-function cutoff that equals 1 if no sliding event has been recorded on contact i over the whole deformation window $\epsilon_1^{init} \rightarrow \epsilon_1^{init} + \delta\epsilon_1$, and 0 otherwise. The first two moments $Q(\delta\epsilon_1) = \langle Q_{\epsilon_1^{init}}(\delta\epsilon_1) \rangle$ and $\chi_4(\delta\epsilon_1) = N_c [\langle Q_{\epsilon_1^{init}}(\delta\epsilon_1)^2 \rangle - \langle Q_{\epsilon_1^{init}}(\delta\epsilon_1) \rangle^2]$ of $Q_{\epsilon_1^{init}}(\delta\epsilon_1)$ (calculated from sample-to-sample fluctuations) are then computed in the quasi-static region ($\tau < \tau_c$). Like this, we evaluate from an initial configuration the number and the associated spatial heterogeneity of sliding events nucleation as axial deformation increases. Figure 5 shows $\langle Q(\delta\epsilon_1) \rangle$ and $\langle \chi_4(\delta\epsilon_1) \rangle$, where $\langle . \rangle$ here means an average over all the values of Δ (since no significant variation of $Q(\delta\epsilon_1)$ and $\chi_4(\delta\epsilon_1)$ is observed in the quasi-static region) computed by considering separately the major and minor force networks. The major force network is defined by selecting contact force greater than the average. By construction, $\langle Q(\delta\epsilon_1) \rangle$ is initially equal to 1. As $\delta\epsilon_1$ increases, $\langle Q(\delta\epsilon_1) \rangle$ decreases but never reaches 0, meaning that a considerable amount of contacts never slides. When considering the whole test, about 35% (respectively 55%) of the contacts of the minor (respectively major) network didn't slide at the end of the test, meaning that the permanent deformation is extremely localized and that rigid bodies remain throughout the whole test [21]. The value of $\langle \chi_4(\delta\epsilon_1) \rangle$ indicates, with respect to increasing axial deformation, the variability in the nucleation of new contact slidings. At low values of $\delta\epsilon_1$, it increases as $\langle \chi_4(\delta\epsilon_1) \rangle \sim \delta\epsilon_1^\beta$ with $\beta = 1.8$, meaning that spatially correlated sites of contact sliding events are nucleating. As $\delta\epsilon_1$ exceeds the threshold value $\delta\epsilon_p = 1.10^{-5}$, $\langle \chi_4(\delta\epsilon_1) \rangle$ saturates, as all the spatially correlated contacts located close to the coulomb criteria, i.e. susceptible to slide, have been destabilized. At this stage, only 4% (respectively 3%) of contacts have slid at least one time in the minor (respectively major) network.

To conclude, incremental stress and strain fields are both characterized by a growing correlation length that diverges at the onset of macroscopic instability, which can therefore be identified as a critical point. A similar behavior has been reported in compressive failure of continuous materials [16, 22]. We interpret these stress and strain specific structures as resulting from dynamic stress redistributions induced by local dissipation of elastic energy materialized by contact slidings. At macroscopic instability, a local contact sliding event induces correlated elastic stress perturbations up to the scale of the whole granular assembly. These features can only be observed when carefully examining characteristic timescales for stresses, and macroscopic deformation for strains concentration processes. Thus, a long time memory, probably associated to a slow evolution of the topology, exists in the system, in relation with the growth of l_τ^* and l_γ^* during mechanical loading towards the macroscopic instability, while the spatial multi-scales structure of stress and strain fields have respectively a short time and deformation life.

The last question that arises is to whether a limit in decreasing correlation length l_γ^* on the shear strain field is reached at $\Delta \rightarrow 0$ for values of $\delta\epsilon_1$ much greater than $\delta\epsilon_p$, which would characterize the thickness of a perennial macroscopic shear band potentially formed at the onset of instability. To investigate this, we hypothesize that, close to the critical point ($\Delta \rightarrow 0$), l^* varies as $l_\gamma^* \sim \frac{L_s^\delta}{L_s^\delta \xi^{\alpha_\gamma} + C_\gamma}$ where $\xi = \frac{\delta\epsilon_1 - \delta\epsilon_p}{\delta\epsilon_p}$, L_s is the square root of the sample area and α_γ is an exponent. This hypothesis is checked from a collapse analysis (inset of Figure 4). We find $\alpha_\gamma = 0.7$. This shows that l_γ^* keeps decreasing as the considered deformation window size $\delta\epsilon_1$ is increased, showing that the correlation length only depends on the value of $\delta\epsilon_1$ and that no intrinsic scale of saturation, potentially associated to a shear band thickness, can be identified at the onset of macroscopic instability.

* florent.gimbert@ujf-grenoble.fr

[1] C.-h. Liu, S. R. Nagel, D. A. Schecter, S. N. Coppersmith, S. Majumdar, O. Narayan, and T. A. Witten. Force fluctuations in bead packs. *Science*, 269(5223):513–515, July 1995.

[2] F. Radjai and S. Roux. Turbulentlike fluctuations in quasistatic flow of granular media. *Phys. Rev. Lett.*, 89:064302, Jul 2002.

[3] A. Liu and S. Nagel. Jamming is not just cool any more. *Nature*, 396:21–22, 1998.

[4] D. Bi, J. Zhang, B. Chakraborty, and R.P. Berhinger.

Jamming by shear. *Nature*, 480:355–358, Dec 2011.

[5] G. Combe and J.N. Roux. Strain versus stress in a model granular material : a devil’s staircase. *Phys. Rev. Lett.*, 85:3628–3631, 2000.

[6] O. Pouliquen and F. Chevoir. Dense flows of dry granular material. *C.R. Physique*, 3:163–175, 2002.

[7] J. Desrues and G. Viggiani. Strain localization in sand: an overview of the experimental results obtained in grenoble using stereophotogrammetry. *Int. J. Numer. Anal. Meth. Geomech.*, 28:279–321, 2004.

[8] J.W. Rudnicki and J.R. Rice. Conditions for the localization of deformation in pressure-sensitive dilatant materials. *J. Mech. Phys. Solids*, 23:371–394, 1975.

[9] B.C. Haimson and J.W. Rudnicki. The effect of the intermediate principal stress on fault formation and fault angle in siltstone. *J. Struct. Geol.*, 32:1701–1711, 2010.

[10] See supplementary material.

[11] F. Radjai and F. Dubois. *Discrete Numerical Modeling of Granular Materials*. Wiley-ISTE, 2011.

[12] P.A. Cundall and O.D.L. Strack. A discrete numerical model for granular assemblies. *Géotechnique*, 29:47–65, 1979.

[13] G. Combe and J.N. Roux. Discrete numerical simulation, quasi-static deformation and the origins of strain in granular materials. *Deformation Characteristics of Geomaterials, 3me Symposium sur le Comportement des sols et des roches tendres, Lyon, 22-24 Septembre 2003, In di Benedetto et al.*, pages 1071–1078, 2003.

[14] G.D.R. Midi. On dense granular flows. *Europhys. Rev. Lett.*, 14:341365, 2004.

[15] D. Marsan, H. Stern, R. Lindsay, and J. Weiss. Scale dependence and localization of the deformation of arctic sea ice. *Phys. Rev. Lett.*, 93(17):178501, Oct 2004.

[16] L. Girard, D. Amitrano, and J. Weiss. Failure as a critical phenomenon in a progressive damage model. *J. Stat. Mech.*, 2010(01):P01013, 2010.

[17] the invariant x , where x represents τ for the shear stress field or γ for the shear strain field, is computed as $x = x_I - x_{II}$, where x represents σ for stress or ϵ for strain, and δx_I and δx_{II} are the principal components of the stress or strain tensor.

[18] E. DeGiuli and J. McElwaine. Laws of granular solids: Geometry and topology. *Phys. Rev. E*, 84(041310):1–9, 2011.

[19] A. R. Abate and D. J. Durian. Topological persistence and dynamical heterogeneities near jamming. *Phys. Rev. E*, 76(2 Pt 1):1–9, 2007.

[20] A. S. Keys, A. R. Abate, S. C. Glotzer, and D. J. Durian. Measurement of growing dynamical length scales and prediction of the jamming transition in a granular material. *Nature Phys.*, 3:260–264, 2007.

[21] K. Szarf, G. Combe, and P. Villard. Polygons vs. clumps of discs: a numerical study of the influence of grain shape on the mechanical behaviour of granular materials. *Powder Tech.*, 2008:279–288, 2011.

[22] L. Girard, J. Weiss, and D. Amitrano. Damage-cluster distributions and size effect on strength in compressive failure. *Phys. Rev. Lett.*, 108:225502, 2012.